International Journal of Chemical Studies

P-ISSN 2349–8528
E-ISSN 2321–4902
IJCS 2015; 2(5): 12-21

Received: 15-12-2014
Accepted: 04-01-2015

Reenu Jacob
Department of Physics,
CMS College, Kottayam, India

Jayakumari Isac
Centre for Condensed Matter,
Department of Physics,
CMS, College, Kottayam, India

Correspondence:
Reenu Jacob
Department of Physics,
CMS College, Kottayam, India

X-ray diffraction line profile analysis of Ba $Sr_{0.6}$ $Fe_{0.4}$ TiO_3 (BSFTO)

Reenu Jacob and Jayakumari Isac

Abstract
BSFTO nanoparticles prepared by solid state technique are characterized by X-ray diffraction analysis (XRD) and SEM. The crystallite development in the BSFTO is investigated by X-ray peak broadening methods like Scherrer method, Williamson Hall (W-H) plot analysis and Size -Strain plot method. The contributions of dislocation density due to crystallite size are also evaluated. A well defined peroskvite phase with tetragonal system is observed from the XRD data. The results showed that the mean crystallite size of the BSFTO estimated from the different methods are highly inter correlated. SEM data revealed that BSFTO has nano crystallite size and EDAX spectrum confirmed its elemental composition.

Keywords: BSFTO($BaSr_{.6}Fe_{.4}TiO_3$), Peroskvites, Debye Scherrer, Williamson-Hall, Dislocation density

1. Introduction
Barium strontium titanate (BST) with high dielectric constant have gained much attention as materials for environmental applications (dielectric for capacitors, actuators, etc.). This perovskite-based ferroelectric, is one of the most studied, exhibiting normal first- order phase transition behaviour. It was previously reported that in Fe-doped (Ba1–xSr x)TiO_3 micro-structural and dielectric properties were modified by controlling the Fe concentration with fixed Sr concentrations [1-9]. Earlier reports on the dielectric properties of BaxSrl–xTiO3 ceramic solid solutions have shown that the compositions exhibited normal ferroelectric behaviour and the loss factor in these materials is reduced with the addition of a proper substitute or doping. Few authors have reported the substitution of Fe in BST where Fe_3+ ion substitutes Ti4+ in BST which reduces the dissipation factor due to domain wall motion [10-12].
A characteristic feature of all solid-state reactions is that they involve the formation of product phase(s) at the interfaces of the reactants. The solid-state reactions initiated by intensive milling in high-energy ball mills could be a good choice for the ceramic powder preparation. An important advantage for intensive milling is the formation of highly dispersed phased materials typical for metal powders or oxide based materials (mechanical activation) or the formation of a new product because of a solid-state reaction [1, 2].
In the present work the authors describes the synthesis and characterisation of BSFTO, a lead free material since they are now at the top as ferroelectric and piezoelectric materials [5]. This nanocrystalline ceramic material is characterized to show good quality and homogeneity. The diffraction patterns of a ceramic sample shows the imperfections in the material like dislocations, small crystallite size, micro strains within the grains due to dislocations and stacking faults. The X-ray diffraction (XRD) peak is broadened due to small crystallite size and strain is due to dislocations and stacking faults. Line profile analysis (LPA) refers to the analysis of the shape of the peaks. Dislocation density (δ) an important material property, which gives the length of the dislocations present per unit volume (m/m3) of the sample. This strongly affects the out-of-pile and in-pile properties of materials [1].
Crystallite size and morphology play important roles in the applications, which drives the modern studies to focus on the synthesis of new nano crystalline materials.

2. Experimental methods.
The new ceramic sample $BaSr_{0.6}Fe_{0.4}TiO_3$ is prepared by the solid state reaction technique using a high-energy ball milling process through mechanically assisted synthesis. For preparing sample, the reagent grade chemicals of high purity Barium Carbonate, Strontium Carbonate, Ferric Oxide and Titanium dioxide powders were used as the raw materials and weighed according to their molecular formula.

The sample was ball milled for three weeks with suitable zirconium balls to insure homogeneity and quality. Then it was attrition milled for three hours. After milling the material was calcined at three different temperatures, 30 ˚C, 850 ˚C & 950 ˚C in a special furnace with oxygen flow arrangements. High temperature is needed for metal oxide phase transformation. The milling conditions are the following: ball-to-powder weight ratio was 40:1 in air atmosphere, basic disc rotation speed was 317/min, rotation speed of disc with jars was 396/min, and the milling time was 32 hrs. After milling the material is heated up to 950 ◦C in a furnace. The temperature of the furnace is increased in steps. High temperature is needed for metal oxide phase transformations. Control of temperature is often necessary to ensure that the desired crystalline phase is formed with optimum particle size [13]. After calcinations, on cooling oxygen flow is allowed into the furnace at fixed intervals (Oxygen Annealing).

X-ray Diffraction pattern for three different temperatures for the sample BSFTO was taken using Bruker AXS D8 advance diffractometer. The diffractometer with radiations of wavelength 1.541A˚ having Nickel filter, equipped with X-ray generator 1140/90/96 having X-ray source KRISTALLOFLXE 780, KF, 4KE with wide angle goniometer PW1710/70 with single pen recorder pm 8203 and channel control PW1390 at 35kV, 10 mA is used for the purpose. The scanning speed of the specimen is 2 degree/minute. From the XRD results, it was concluded that this crystal was found to be tetragonal system. The different methods used to evaluate the crystallite size of the sample are given below.

2.1. Scherrer method

X-ray diffraction profile is used to measure the average crystallite size of the sample provided the average diameter was less than 200 Å. The lines in a powder diffraction pattern are of finite breadth but since the particles were very small, the lines started to broaden than usual. The broadening decreases with the increase in crystallite size. The crystallite size for $BaSr._6Fe._4TiO_3$ is calculated from X-ray diffraction profiles of strong reflections with intensity % by measuring the full width at half maximum (FWHM). The Debye Scherrer equation for calculating the crystallite size is given by

$$\boldsymbol{D = \frac{K\lambda}{\beta cos\theta}} \quad (1)$$

Where, K is the Scherrer constant, λ is the wavelength of light used for the diffraction, β the "full width at half maximum" of the sharp peaks, and θ the angle measured. The Scherrer constant (K) in the above formula accounts for the shape of the particle and is generally taken to have the value 0.9. The results revealed that the crystallite size is less than 100 nm. The XRD diffraction profile of the sample BSFTO at temperatures 30 ◦C, 850 ◦C & 950 ^{0}C are given below in Fig. 1

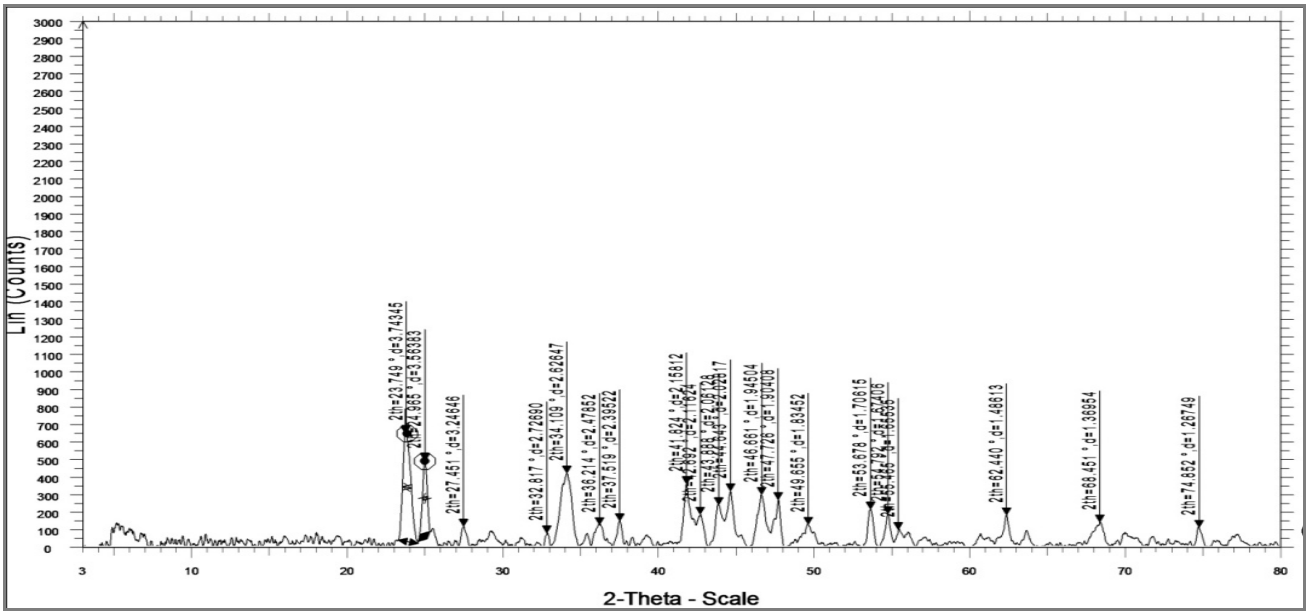

(a)

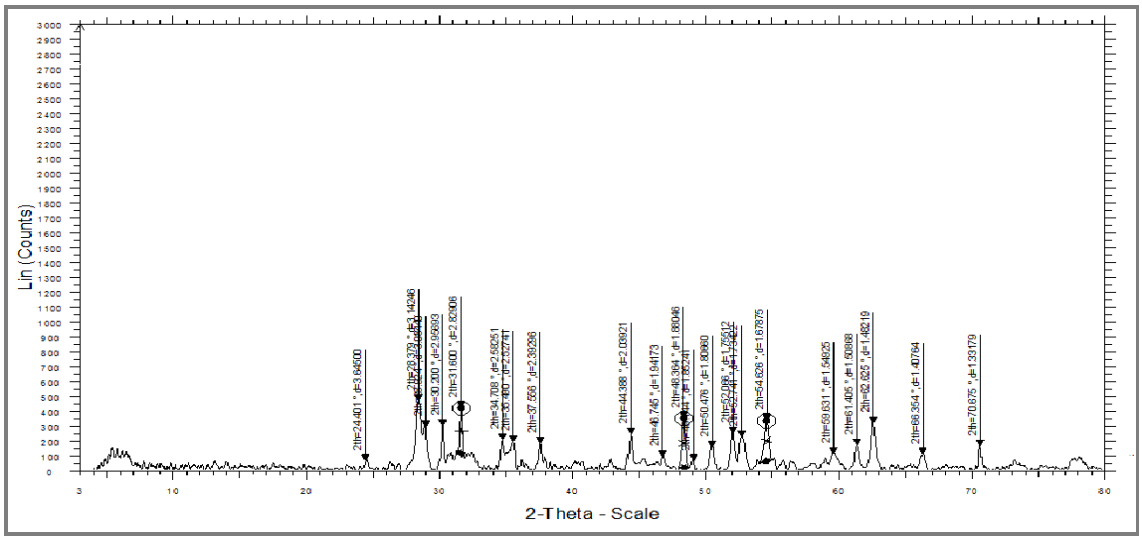

(b)

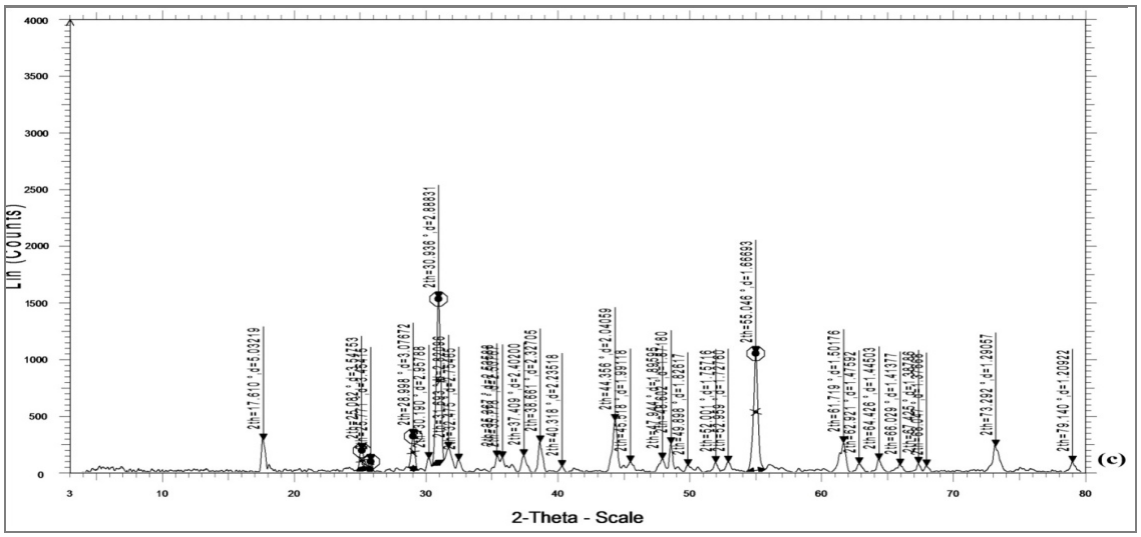

Fig 1: shows the XRD diffraction profile of the sample BSFTO at temperatures 30 ◦C, 850 ◦C & 950 ◦C.

a = b ≠ c and α = β = γ = 90˚.
a =10.2177**A**◦**, b = 10.2177**A◦**, c** = 5.5167**A◦.**

Table 1: The (hkl) indices calculated from the 2θ values of the XRD profile are listed below.

2θ in degrees	hkl
30.936	(115)
32.472	(106)
35.267	(302)
40.318	(304)
44.356	(314)
52.001	(316)
55.046	(414)
61.719	(0011)

XRD data can be analysed to study the peak broadening with crystallite size. Crystals formed may not be perfect due to their finite size. The disparity or deviations from perfect crystallinity leads to the broadening of the diffraction peaks. The two main factors of peak width analysis are the crystallite size and lattice strain. Hence the 2θ peak positions get shifted. The breadth of the Bragg peak is a combination of both instrument and sample dependent effects as

$$\beta^2_{\text{crystallite size}} = \beta^2_{\text{measured}} - \beta^2_{\text{instrumental.}}$$

Therefore D = K λ / β cos θ => cos θ K λ/D(1/ β) ----- (2).

2.2 Scherrer plot method

Scherrer Plots were drawn with 1/ β on the X-axis and Cos θ along the Y-axis at different temperatures as given in the Fig. 2.

By linear fitting the data, the crystallite size D was extracted from the slope of the line.

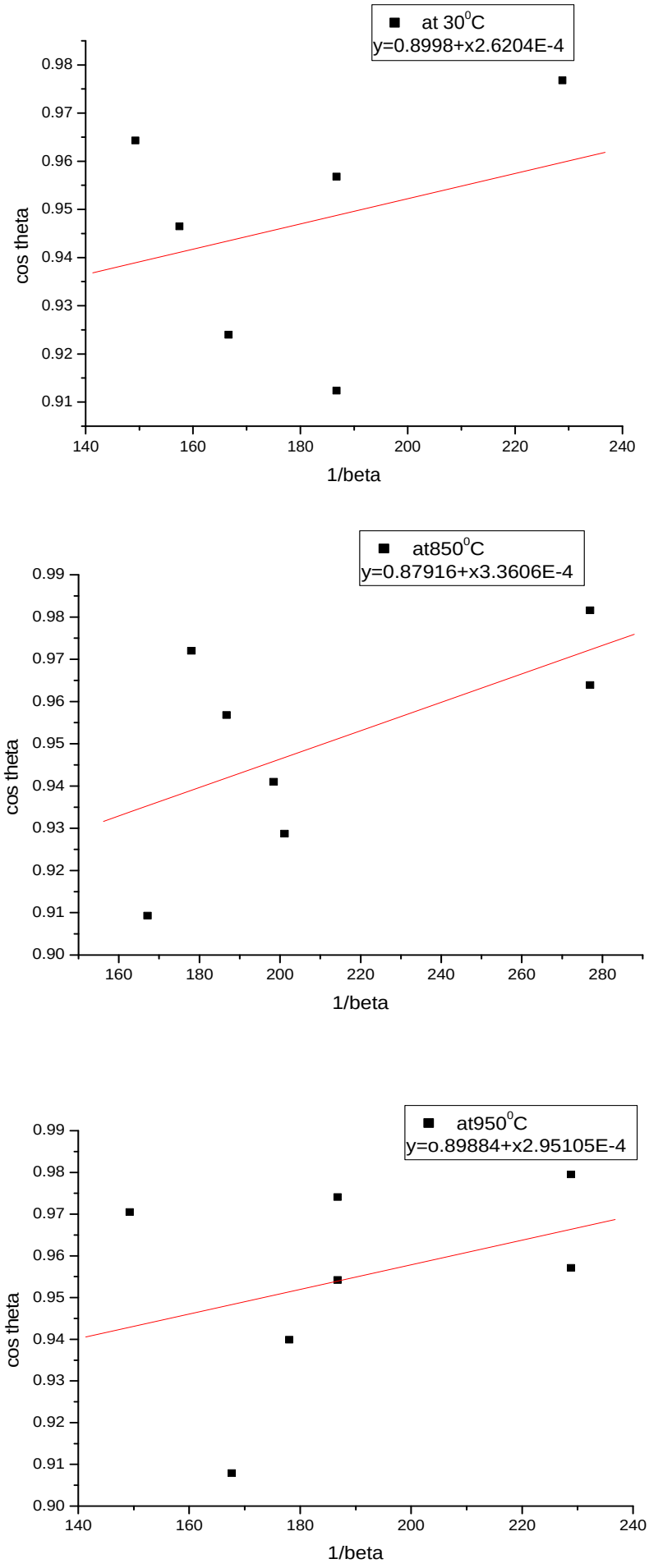

Fig 2: shows the Scherrer plots of BSFTO at different temperatures.

2.3 Wiliamson- Hall (W-H) Plot method.

W-H plots emphasised the strain induced plots. The peak width derived from crystallite size varies as 1/cos θ whereas strain varies as tan θ. This difference in behaviour as a function of 2θ enables to distinguish between the size and strain effects on peak broadening. The Bragg width contribution from crystallite size is inversely proportional to the crystallite size [16]. W-H analysis is a simplified integral breadth method where size-induced and strain-induced broadening are deconvoluted by considering the peak width as a function of 2θ [14].

Addition of Scherrer formula and the strain induced broadening results in

$\beta^2_{hkl} = K\lambda/D\cos\theta + 4\varepsilon \tan\theta$ ------(3) **where ε** represents the strain.

W-H plots are drawn with β cos θ along the Yaxis and 4sin θ along the X axis as given in Fig. 3. The slope and Y-intersect of the fitted line represent strain and particle size, respectively.

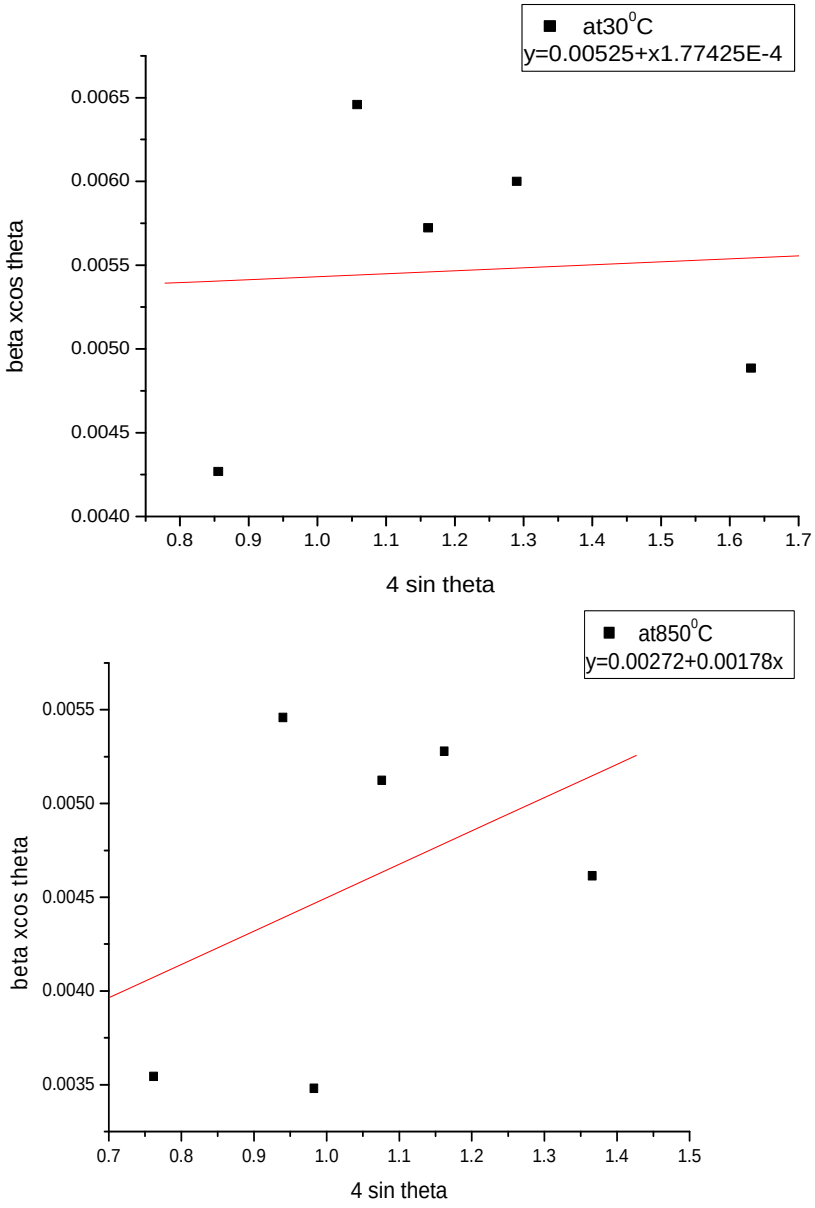

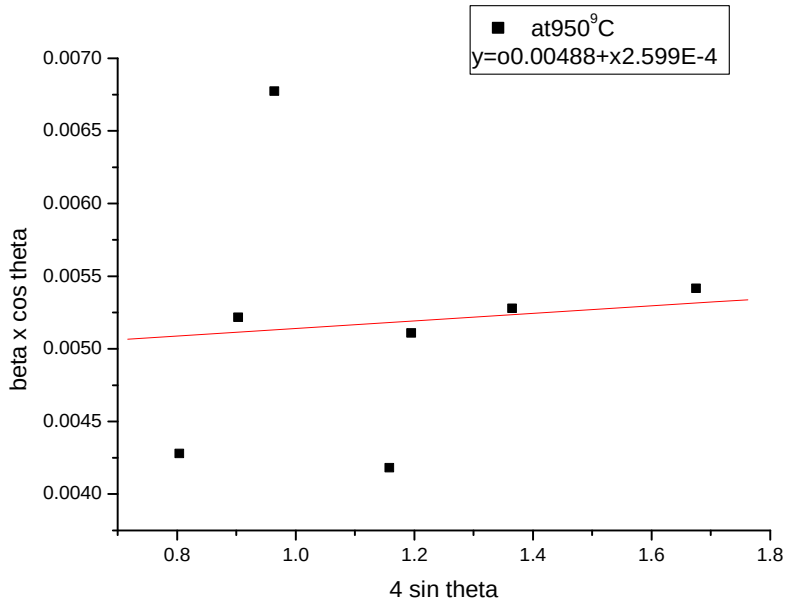

Fig 3: represents the W-H plots of BSFTO at different temperatures.

2.4 Size-Strain Plot Method

The value of d (the inter planar spacing between the atoms) is calculated using the

Bragg's Law, $2d\sin\theta = n\lambda$ or

$$d = \frac{\lambda}{2\sin\theta n(n=1)} - - - - (2)$$

Wavelength of X ray = 1.5 Å for CuKα.

Williamson-Hall plot has explained that line broadening was basically isotropic. Due to micro strain contribution the diffracting domains are also isotropic. Size-strain parameters can be obtained from the"Size-Strain Plot" (SSP). Here it is assumed that the 'strain profile' is given by Gaussian function and the 'crystallite size' by Lorentzian function [15].

In the plots given below in Fig. 4, $d^2_{hkl}\,\beta_{hkl}\cos\theta$ and $(d_{hkl}\,\beta_{hkl}\cos\theta)^2$ were taken on X- axis and Y-axis respectively for all peaks. The crystallite size is calculated from the slope of the linearly fitted data and the root of the Y-intercept gives the strain [15].

The crystallite size D can be measured from the Debye Scherrer formula as $D=0.9\lambda/\beta\cos\theta$.

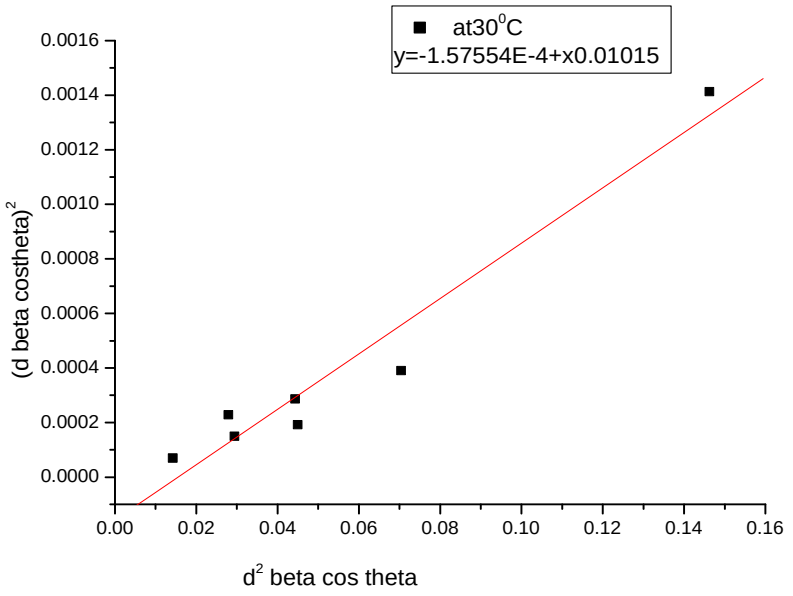

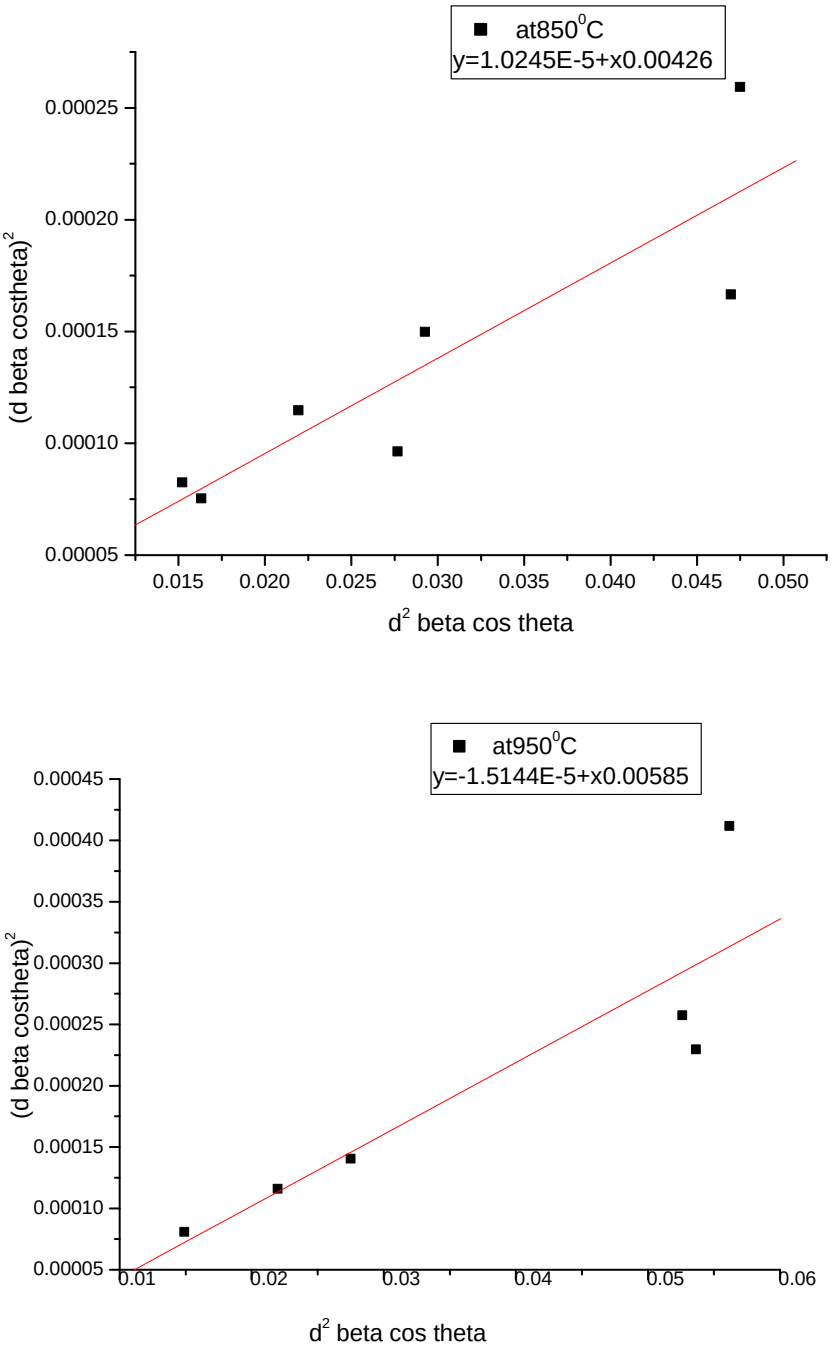

Fig 4: $(d^2_{hkl}\,\beta_{hkl}\,\cos\theta)$ versus $(d_{hkl}\,\beta_{hkl}\,\cos\theta)^2$ plots are given.

Table 2: The crystallite size of the sample BSFTO calculated from the different methods are listed below.

Sample at Different Temperatures	2θ in degrees	Scherrrer Method		W-H Plot Method		Size –Strain Analysis Method	
		By equation	by plot analysis	crystallite size	strain	crystallite size	strain
30 ◦C	23.749 24.965 41.824 53.678	13.798 nm 25.00 nm 23.06 nm 23.96 nm	23.44 nm	25.24	0.00423	13.65 nm	.0077
850 ◦C	24.401 30.200 44.288 54.626	39.08 nm 25.38 nm 27.05 nm 25.54 nm	27.89 nm	35.53 nm	0.003846	32.53 nm	0.0077

950 ◦C	25.082 30.996 44.355 55.046	32.38 nm 20.46 nm 26.25 nm 25.44 nm	27.51 nm	27.17 nm	0.003523	23.69 nm	.00707

2.5 XRD- Dislocation density

The dislocation density is defined as the length of dislocation lines per unit volume of the crystal. Chen and Hendrickson measured and determined dislocation density and hardness of several crystals. Theoretically a dislocation is a crystallographic irregularity or a defect formed within the crystal. The properties of the crystal formed are strongly influenced by the defects inside the crystal. Shift or movement of a dislocation is impeded by other dislocations present in the sample. They found that crystals with larger dislocation density were harder. It has been shown that the dislocation density increases while crystallite size decreases with increasing strain and ultimately these parameters reach saturation values. Above a certain crystallite size limit (~20 nm) the strength of materials increases with decreasing crystallite size. The dislocation density (δ) in the sample has been determined using values of FWHM, θ, lattice constant and crystallite size. The number of unit cell is calculated from crystallite size and cell volume of the sample [16].

(δ)= 15βcosθ/4aD, where **β,** the FWHM measured in radians**, θ** the diffracting angle, **a** the cell parameter and **D** is the crystallite size in nm. The no. of unit cells**, n=π x(4/3)(D/2)^3 x1/V**, where **V** is the cell volume of the sample(V=575.9531A ◦^{3}).

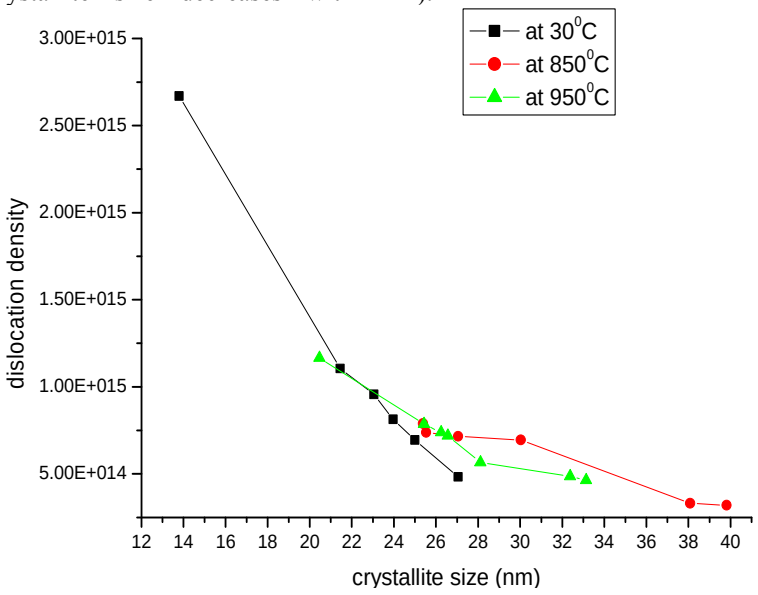

Fig 5 (a): The variation of dislocation density **(δ)** with the crystallite size and no. of unit cells are given below

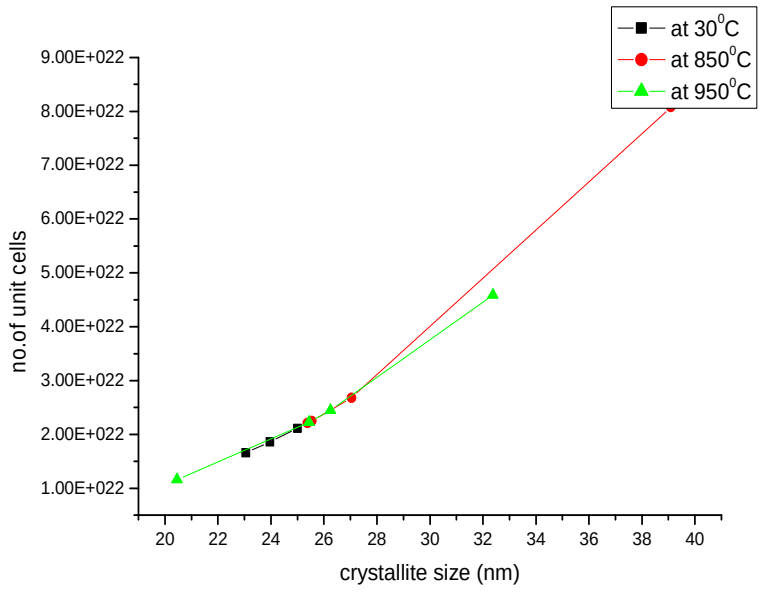

Fig 5 (b): dislocation density dependence with no. of unit cells and crystallite size of the sample BSFTO.

2.6 SEM Analysis

The SEM analyses the surface of solid objects, producing images of higher resolution than optical microscopy and

produces representations of the sample under study. Fig. 6 shows the surface morphology of BSFTO. The crystallite size measurement through SEM revealed that its maximum dimension is always less than 100 nm. SEM images shows that the iron concentration induces a strong effect of exaggerated grain growth formation and hence large faceted grains sample results. Thus dominant XRD peaks of new hematite phase appears at high temperature.

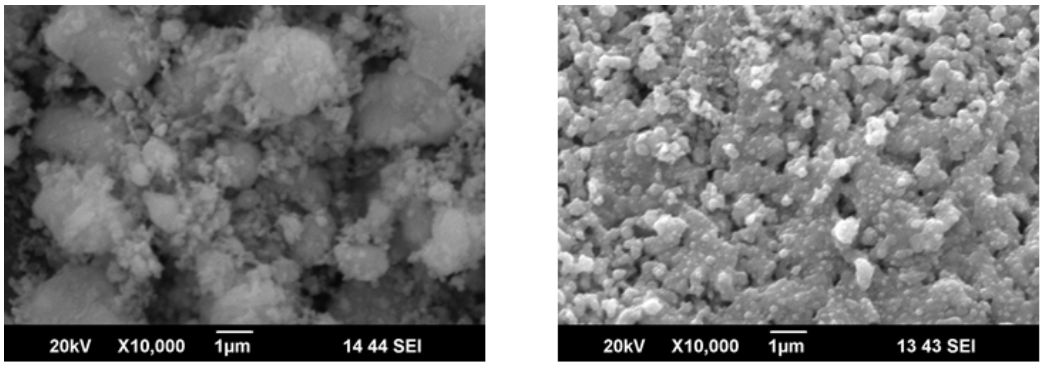

Fig 6: Surface Morphology of BSFTO.

2.7 Energy Dispersed X-Ray Spectrograph (EDX)

EDAX shows the composition details of the prepared ceramic powders. (Fig. 7). The instrument used for this measurement is ISIS Link Oxford Instrument UK. This technique is generally associated with Scanning Electron Microscope (SEM). The size of the pulse generated depends on the number electron hole pairs created, which in turn depends on the energy of the incoming X-ray. In this method however elements with low atomic number are difficult to be detected. The detector which is lithium doped silicon is protected by a beryllium window and operated at liquid nitrogen temperatures.

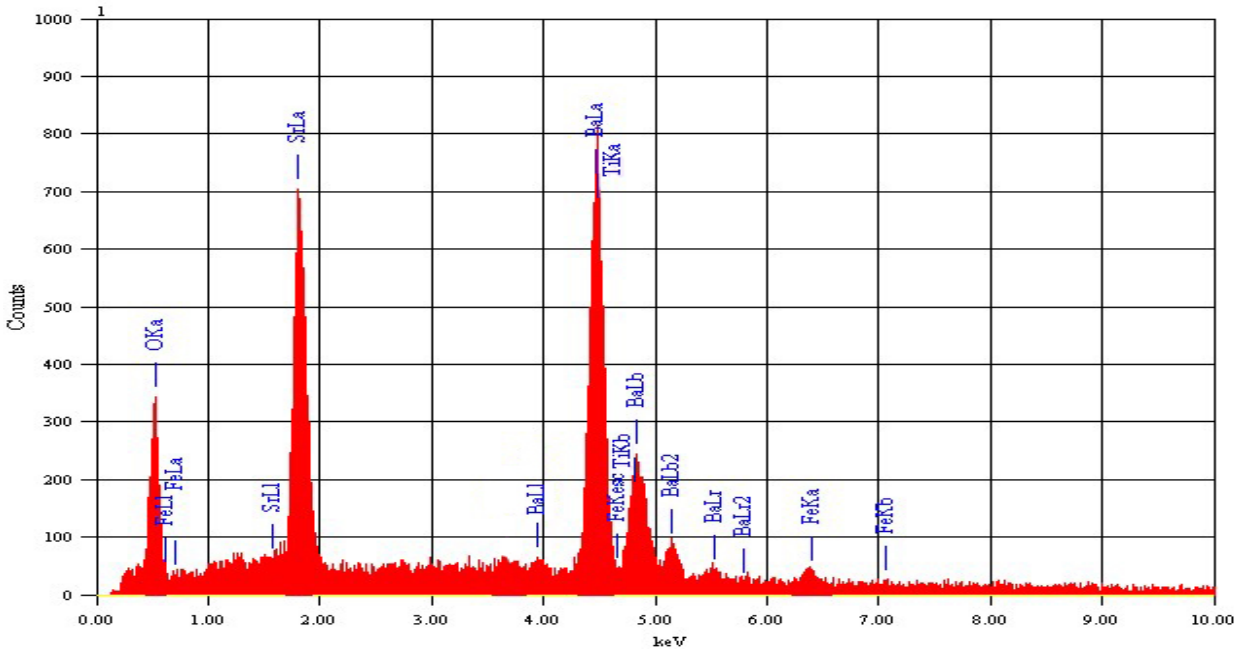

Fig 7: EDAX spectrum of BSFTO

From the EDAX spectrum, the four dominant peak positions at 4.465keV (Ba Lα), 5.1,.5,5.8keV (Ba Lβ, Lγ, Lγ2), 1.806keV (Sr Lα), 0.705, 6.398keV (Fe Lα, Kα), 0.452, 4.508keV (Ti Lα, Kα), 0.525keV (O Kα) correspond quite well to the energy pattern of the corresponding materials (Ba, Sr, Fe, Ti, and O) reported in the EDAX international chart.

3. Results and Discussion

In the present work a systematic and detailed study of the new lead free ceramic BSFTO ($BaSr_{.6}Fe_{.4}TiO_3$) was successfully done. Line Profile Analysis of the sample was carefully carried out to analyse the shape of the diffraction peaks.

The XRD patterns of BSFTO sample obtained for various annealing temperatures are shown in Figure 1. XRD spectrum gave a clear idea about the maximum intensity peak shifting corresponds to the different treating temperatures. As the temperature increases, the highest peaks in the XRD spectrums shifts from left to right through the 2θ axis.

The atoms undergo thermal vibration about their mean positions even at the absolute zero of temperature, and the amplitude of this vibration increases as the temperature increases. Increased thermal vibration of the atoms, as the result of an increase in temperature, the unit cell expands, causing changes in d spacing and therefore in the 2θ positions of the diffraction lines. And also the intensities of the diffraction lines decrease. When the material is cooled to room temperature, the amplitude of the atomic vibrations of the material was decreased. But it couldn't arrive at the initial

amplitude. The atomic vibration amplitude of the heated material was higher than initial amplitude [13].

From Fig. 1, the peak broadening in the XRD patterns clearly indicated the nature of formation of the very small nano ceramic material. From the width of the XRD peak, the mean crystallite size is calculated using Debye Scherrer's equation. The values calculated using the Scherrer formula are compared to the values obtained through Scherrer plot, Williamson-Hall plot and the Size-Strain Plot drawn for various temperatures. The disparity or deviations from perfect crystallinity leads to the broadening of the diffraction peaks and hence the 2θ peak positions get shifted. Results obtained from different methods are in good agreement. For the size strain plots negative strain is also observed which can be accounted as the lattice shrinkage.

From Table 1, it is confirmed that crystallite size of the material BSFTO increases with the treating temperature increase. The diffraction data revealed that the material belongs to tetragonal system. Heat treatment causes the particles to anneal and form larger grains, which of course indicates that the particles become larger. Hence, the large size of sample at 850 ˚C is expected. But as the temperature is increased the crystallite size reduces slightly. This can be explained as the fact that the crystallite growth was hindered by the oxygen vacancies, lattice distortion as well as the internal stress arising from the substitution of Fe [1]. As the Fe concentration increases properties of the material is enhanced. The hkl values calculated from the XRD profile are listed in the Table.2.

The dislocation density (δ) is determined from the XRD profile. It is clearly confirmed that dislocation density decreases as the crystalline size increases. Higher value of dislocation density results in greater hardness. The no. of unit cells also is found to have an inverse relation with the dislocation density.

Figure. 6 shows SEM image of BSFTO. The SEM photograph revealed that maximum dimensions of the particles are less than 100 nm. This is an experimental proof of the theoretical calculation of crystallite size by Debye Scherrer equation. SEM images clearly shows that with the addition of iron a strong effect of exaggerated grain growth results which again leads to the formation of large faceted grains. This can be confirmed with the dominant XRD peaks of the sample in which new hematite phase appearing at higher temperature [17]. Thus the morphology of particles has changed from irregular to spherical and finally facetted shape [17].

The EDAX spectrum (fig. 7) obtained give the confirmation of the elemental composition of the material under investigation. The EDAX analysis indicates that the elements exist in the sample and they agree with the chemical formula of the prepared compound. A sound understanding of the properties of sample shows that BSFTO will definitely have a future in power electronics.

4. Conclusion

The new nano ceramic material BSFTO ($BaSr_{.6}Fe_{.4}TiO_3$) prepared using the solid state technique is characterized by XRD and SEM analysis. The XRD line profile analysis indicated the formation of a peroskvite phase at high temperature. The line broadening effect showed a decrease in crystallite size and lattice strain. The mean crystallite size increases at first but shows slight decrease as the temperature is increased. The results of broadening analysis by Scherrer plot method, W-H plot method and Size-Strain plot method are in high inter correlation. SEM results also agrees well with the results of W-H and SSP methods.

5. Acknowledgement

The authors are thankful to SAIF, Kochi for providing the data analysis and to the Principal, CMS College, Kottayam, Kerala for providing the facilities.

6. References

1. Willander O, Nur M, Israr Q, Hamad ABA, El Desouky FG, Salem MA *et al*. Determination of A.C. Conductivity of Nano-Composite Perovskite Ba(1–x–y)Sr(x)TiFe(y)O_3 Prepared by the Sol-Gel Technique M. Journal of Crystallization Process and Technology, 2012, 2, 1-11 Published Online January 2012. (http://www.SciRP.org/journal/jcpt, 22 Jan, 2015.
2. Battisha K, Hamad ABA, Mahani RM. Structure and Dielectric Studies of Nano-Composite Fe_2O_3: $BaTiO_3$ Prepared by Sol-Gel Method. Physica B, 404, 16, 2009, 2274-2279.
3. Lin F, Shi W. Effect of Sr Concentration on Micro-structure and Magnetic Properties of (Ba1−xSrx) (Ti0.3Fe0.7) O_3 Ceramics. Journal of Magnetism and Magnetic Materials 2010; 322(14):2081-2085.
4. Wei X, Xu G, Ren Z, Wang Y, Shen G, Han G. Size-Controlled Synthesis of $BaTiO_3$ Nanocrystals via a Hydrothermal Route. Materials Letters 2008; 62(21-22):3666-3669.
5. Sundaresan A, Rao CNR. Ferromagnetism as a Universal Feature of Inorganic Nanoparticles, Nano Today 2009 Vol 4(1):96-106.
6. Hsing HI, Hsib CS, Huang CC, Fu SL. Low Temperature Sintering and Dielectric Properties of Ba-TiO3 with Glass Addition. Materials Chemistry and Physics 2009; 113(2-3):658-663.
7. Kong LB, Zhang TS, Ma J, Boey F. Progress in synthesis of ferroelectric ceramic materials via High Energy Mechanochemical Technique. Progress in Materials Science 2008; 53(2):207-322.
8. Roscher M, Schneller T, Waser R. Sol-Gel Sci J Tech 56, 2010, 236.
9. Shao Z, Xiong G, Tong J, Dong H, Yang W. Ba Effect in Doped Sr(Co0.8Fe0.2)O3-δ on the Phase Structure and Oxygen Permeation Properties of the Dense Ceramic Membranes. Separation and Purification Technology, Vol. 25, No. 1-3, 2001, 419-429.
10. Mao C, Dong X, Zeng T, Chen H, Cao F. Ceramics International 2008, 34:45.
11. Kavian R, Saidi A. Sol-Gel Derived BaTiO3 Nano-Powders. Journal of Alloys and Compounds 2009; 468(1-2):528-532.
12. Jacob R, Isac J. Optical constants and dispersion parameters of $BaSr_{0.6}Fe_{0.4}TiO_3$. International Journal of Recent Scientific Research 2014; 5(11):2067-2071.
13. Vinila VS, Jacob R, Mony A, Nair HG, Issac S, Rajan S. XRD Studies on Nano Crystalline Ceramic Superconductor PbSrCaCuO at Different Treating Temperatures. Crystal Structure Theory and Applications 2014; 3, 1-9.
14. Zak AK, Majid WHA, Abrishami ME, Yousefi R. X-ray analysis of ZnO nanoparticles by WilliamsoneHall and sizeestrain plot Methods. Solid State Sciences 2011; 13:251e256.
15. Prabhu YT, Rao KV, Kumar VSS, Kumari BS. X-ray Analysis of Fe doped ZnO Nanoparticles by Williamson-

Hall and Size-Strain Plot Methods. International Journal of Engineering and Advanced Technology (IJEAT) 2013; 2(4):2249–8958.
16. Devamani RHP, Rani JM. Synthesis and Characterization of Lead Chromate nanoparticles. IJSR 2014; 3(4):2277-8179.
17. Habiba A, Haubnerb R, Stelzer N. Effect of temperature, time and particle size of Ti precursor on hydrothermal synthesis of barium titanate. Materials Science and Engineering B 2008;152:60–65.